Article

High Frequency Transformer's Parasitic Capacitance Minimization for Photovoltaic (PV) High-Frequency Link-Based Medium Voltage (MV) Inverter

Himanshu [1], Harsimran Singh [2], Pandiyan Sathish Kumar [1], Muhammad Umair Ali [1], **Ho Yeong Lee [1], Muhammad Adil Khan [1], Gwan Soo Park [1] and Hee-Je Kim [1,***

[1] School of Electrical Engineering, Pusan National University, Busandaehak-ro 63 beon-gil 2, Busan 46241, Korea; himanshuhimanshu820@gmail.com (H.); sathishnano2013@gmail.com (P.S.K.); umairali.m99@gmail.com (M.U.A.); hyl@pusan.ac.kr (H.Y.L.); engradilee@gmail.com (M.A.K.); gspark@pusan.ac.kr (G.S.P.)

[2] Institute of Robotics and Mechatronics, German Aerospace Center (DLR), 82234 Wessling, Germany; harsimran.smit@gmail.com

* Correspondence: heeje@pusan.ac.kr; Tel.: +82-51-510-2364

Abstract: The high-frequency-based medium voltage (MV) inverter is used in renewable energy power sources for power transmission. However, power quality is compromised as a result of the increase in common mode noise currents by the high inter-winding parasitic capacitance in high-frequency link transformers. This fast voltage transient response leads to harmonic distortion and transformer overheating, which causes power supply failure or many other electrical hazards. This paper presents a comparative study between conventional and modified toroid transformer designs for isolated power supply. A half bridge high-frequency (10 kHz) MV DC–AC inverter was designed along with power source; a 680 W solar module renewable system was built. An FEM-simulation with Matlab-FFT analysis was used to determine the core flux distribution and to calculate the total harmonics distortion (THD). A GWInstek LCR meter and Fluke VT04A measured the inter-winding capacitance and temperature in all four transformer prototypes, respectively. The modified design of a toroid ferrite core transformer offers more resistance to temperature increase without the use of any cooling agent or external circuitry, while reducing the parasitic capacitance by 87%. Experiments were conducted along with a mathematical derivation of the inter-winding capacitance to confirm the validity of the approach.

Keywords: high-frequency-based MV inverter; transformer's parasitic capacitance; total harmonic distortion; toroidal transformer; sector windings

1. Introduction

A transformer plays a vital role in energy conversion and is at the heart of the electric power system. The transformer size decreases with increasing frequency, which allows for the building of smaller, less expensive, and compact portable electrical devices [1,2]. Therefore, high frequency power transformers are preferred over traditional frequency transformers (50–60 Hz) in the power electronic fields, such as switching power supplies; converters; and inverters, including medium voltage (MV) inverters, which offer a step-up transformer-less solution to interconnect photovoltaic (PV) arrays to the MV grid [3–8].

Green energy is a priority of many researchers because of population and industrial growth, which are leading the world towards an extensive rise of global warming threats and visible climate change. Therefore, renewable energy sources are in high demand, particularly solar and wind energy.

These sources are projected to fulfill 50% of the energy requirement by the year 2050 [9]. On the other hand, the intermittent nature of these power sources is a major limitation to connecting them straight to electrical/electronic systems or national grids. This critical obstacle can be overcome using external devices, such as energy storage, converters, and inverters (see Figure 1) [10–13]. As a result of the high penetration of these high-frequency-based MV inverters into the renewable energy power plants, energy demands could be fulfilled for industries and home power requirements. However, these high-frequency links, for example, high-frequency transformer, H-bridge inverter dead time, and non-linear load, generates high harmonic content. This can cause serious damage to the equipment including overheating, power supply failure, or electric shock hazards [14,15]. Consequently, to protect the component and the connected loads from overheating and to provide a power supply without any disturbances, the power quality of these MV inverters needs to be taken into consideration [16–19].
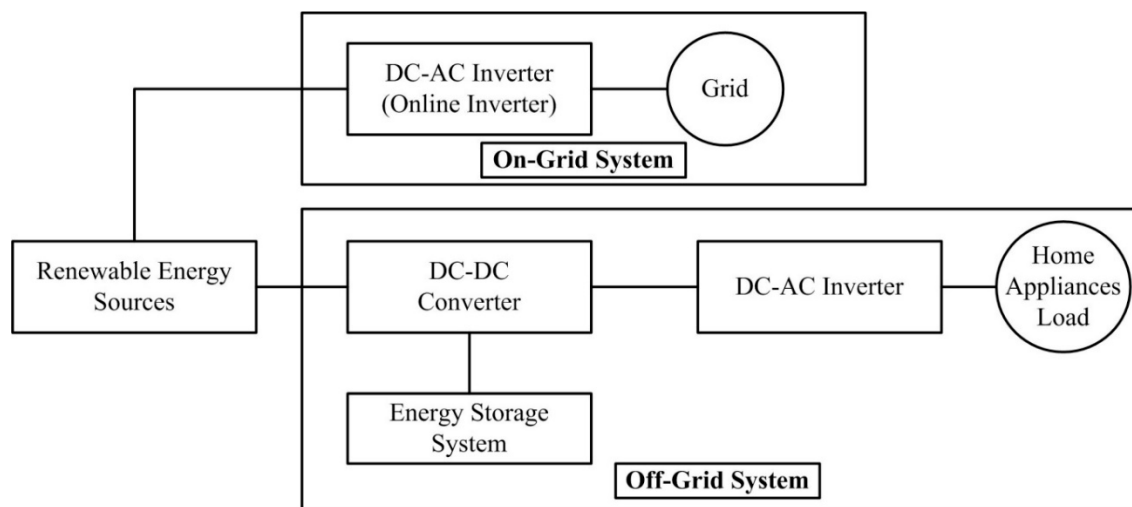

Figure 1. Renewable energy source on and off grid system.

An electromagnetic interference (EMI) in inverters can affect the power quality of transients, both short time and longtime deviation, which can cause harmonics. In these devices, harmonics can be categorized into two classes: common and differential conduction modes (CCM and DCM) [20–22]. The high-frequency transformer is one of the sources of EMI and contributes to the common mode harmonics because of the intrinsic coupling capacitance, and electric and magnetic fields [23]. The duty cycle is inversely proportional to the harmonics. Therefore, DCM operations of pulse-width modulation (PWM) converters increase the harmonics, which adds power losses in transformer windings. Similarly, high-frequency operation causes skin and proximity effects that elevate the harmonic losses, winding power losses, and rapid growth in the operating temperature [24,25]. On the other hand, high frequency winding losses and lowering the leakage inductance has been a major research focus, while the winding capacitance requires equally serious attention during the design of transformers. Capacitive coupling is one of the paths that can carry high frequency noise; premature resonance; electrostatic coupling to other circuits; and fast transient voltages from primary to secondary circuitry, which produces common mode noise currents and an increase in transformer temperature in the device, resulting in a deterioration of the overall system operation, noise, health, and safety threats.

This capacitive coupling is an eruption effect of a transformer parasitic, rooted by a wide range of capacitance across the transformer, which circulates as a result of winding arrangements. Therefore, the key to overcoming this critical hurdle is lowering the inter-winding capacitance. Conventional methods to reduce the emergence of capacitive coupling at the transformer include increasing the insulation between the primary and secondary winding or increasing the distance between the primary and secondary winding by winding them on opposite sides of the toroidal core. These changes in the transformer will, however, cause other drawbacks, such as high leakage inductance, larger physical

size, and poor inductive coupling. Accordingly, conventional methods are not completely effective in improving the power quality. On the other hand, previous studies [26–32] examined the techniques on smart transformers fuzzy logic based transformers by winding using fiber optic sensors and certain oils for cooling the transformer. They, however, were arranged specifically for the coupling capacitance and temperature control and showed no significant difference when compared with the less expensive conventional solutions.

The leakage inductance and primary/secondary capacitance are mutually exclusive and are governed by the distance between the windings and the unwounded core. As a result of this, it is difficult to achieve both low capacitive coupling and a high degree of inductive coupling in a power transformer [33,34]. To circumvent this inherent tradeoff in this study, the conventional toroid ferrite core transformer was modified by an additional 3D printed polylactic acid (PLA) mold, which separates the primary and secondary windings, and helps to implement unique sector winding. Although the distance between windings will introduce leakage inductance, there is some gain in capacitance due to the dielectric constant of PLA. However, the magnetic core geometry and winding arrangements have a large influence on self-capacitance and leakage inductance of the transformer and because of the addition of a mold, it enables access to various types of winding arrangements. This paper reports a comparative analysis on the high frequency-link MV inverter for power-quality improvement by effective subtraction of capacitive coupling and reducing the temperature increase without using any extra circuitry or cooling agents.

2. High-Frequency Link Based MV Inverter Design Consideration

2.1. Toroid Ferrite Core

To utilize the intrinsic ferrite material properties, it is essential to use a ring configuration of the ferrite core. Therefore, the toroid core was used in this paper, as it is commonly used for high-frequency square/sine wave-based applications, such as power input filters, ground-fault interrupters, common-mode filters, and pulse and broadband filters.

A 77 material ferrite toroid was used as the core for MV inverter high-frequency link transformer. Figure 2 presents a schematic diagram of the core and is defined by its outer diameter (A), inner diameter (B), and thickness (C) (See Table 1). Figure 3 shows how the increasing temperature affects the core properties and Table 2 presents toroid ferrite77 core material's electrical properties.
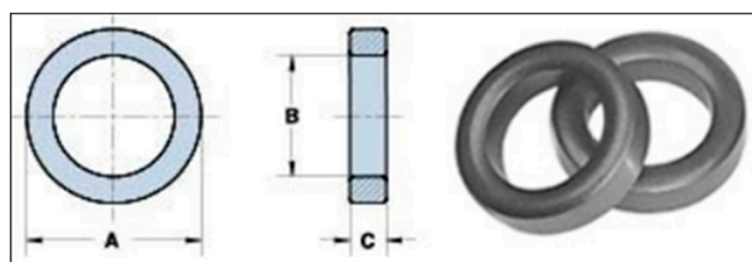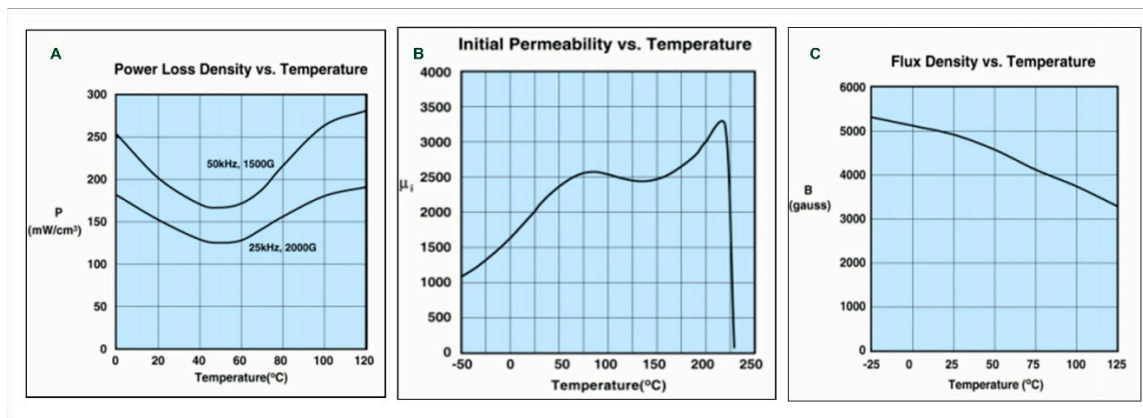

Figure 2. Ferrite 77 material core dimensions (courtesy: Fair-Rite products Corp).

Table 1. Ferrite 77 toroid core dimensions (courtesy: Fair-Rite products Corp).

Dim	mm	Mm tol	Nominal
A	61.00	±1.30	2.400
B	35.55	±0.85	1.400
C	12.70	±0.50	0.500

Table 2. Ferrite 77 toroid core electrical properties (courtesy: Fair-Rite products Corp).

Electrical Properties	
A_L (nH)	$2950 \pm 25\%$
A_E (cm^2)	1.58000
$\sum I/A$ (cm^{-1})	9.20
I_e (cm)	14.50
V_e (cm^3)	22.80000

Figure 3. Temperature effects on Ferrite 77 material properties (courtesy: Fair-Rite products Corp).

2.2. Harmonic Current Contribution on Transformer Losses and Temperature Rise

Total harmonics distortion (THD) is a widely-used notion to define the harmonic content in alternating signals. This value is defined as the ratio sum of the powers of all harmonic components to the power of the fundamental frequency. THD is used for low, medium, and high voltage systems, where the current and voltage distortion is defined as THD_I and THD_V, and can be calculated using the following Equations (1)–(2).

$$THD_v = \left[\left(\sum_{h \neq 1}^{H} |V_h|^2 \right)^{\frac{1}{2}} / |V_1| \right] \times 100\% \tag{1}$$

$$THD_I = \left[\left(\sum_{h \neq 1}^{H} \left| I_i^h \right|^2 \right)^{\frac{1}{2}} / |I_1| \right] \times 100\% \tag{2}$$

where h is the harmonic content order, and V_h and I_h are the voltage and current amplitude of order "h" harmonic component, respectively. V_1 and I_1 are the voltage and current amplitude of the fundamental component, respectively.

The International Electrotechnical Commission (IEC) 61727 imposes the limits for harmonics in the current—Electromagnetic compatibility (EMC)-Part 3–2: Limits for harmonics current emission. The IEEE Single Phase Harmonics Task Force (P1495) has set similar limitations. U.S. and European power systems are different from each other in many standards. Therefore, the United States should be different than the IEC stance. Thus, there is a flexibility to follow the certain standard (Table 3).

Table 3. Current and Voltage total harmonic distortion allowing values and their associated risks (courtesy: Interpreting European norm (EN) 50160 and International Electrotechnical Commission (IEC) standard 61727). THD—total harmonics distortion.

THD_V	THD_I	Risk
<8%	<5%	normal situation considerable
8–15%	5–50%	Minor harmonic pollution with malfunctions possibility
>15%	>50%	major harmonic pollution with malfunctions probability

The losses in transformers can be classified as load loss (impedance loss), no-load loss (excitation loss), and total loss (no-load + load-loss). Load loss can be subdivided further into stray magnetic losses in the core, eddy currents, and resistive losses in the windings.

$$p_t = p_f \sum_{h=1}^{h=h_{max}} I_h^2 h^2 \tag{3}$$

where P_f is the eddy current loss at the fundamental frequency, and f and I_h are the fractions of the total RMS load current at the harmonic number h.

2.3. Circuit Operation

Figure 4 shows, A single-phase half bridge (10 kHz) is comprised of two power MOSFET (IRF 250) (Texas Instruments, Dallas, TX, USA), S1 and S2, which are driven by a DSP F28335 (Texas Instruments, Dallas, TX, USA) chip to generate a pulse width modulated waveform and feedback diodes, D1 and D2. These are called freewheeling diodes with two DC bus capacitors to stabilize the DC voltage. Two-stage power conversions with the help of the high-frequency transformer. High-frequency operation is possible at the first DC/DC stage and at the second stage modified amplitude of converted high-frequency AC voltage by high-frequency transformer secondary, which is connected to high-frequency rectifier AC/DC and an output inverter, which converts the DC voltage to the required frequency AC voltage in the case of utility grid 50/60 Hz.
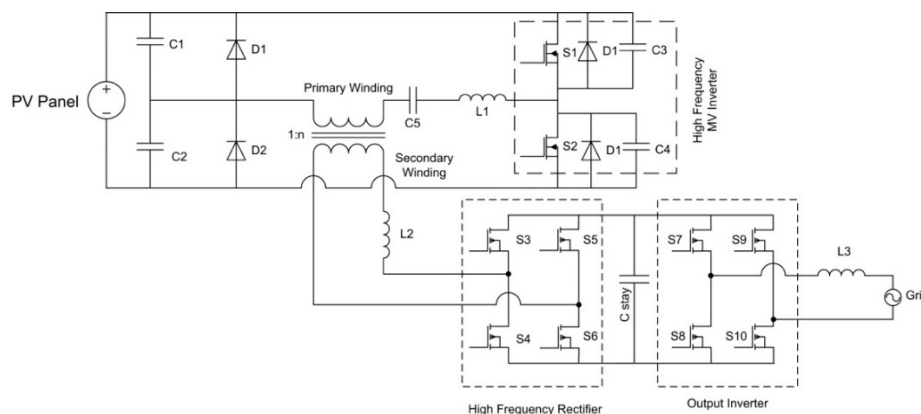

Figure 4. Circuit layout for photovoltaic (PV) high-frequency-based medium voltage (MV) inverter system.

3. Fabrication

This study examined a new design for the high-frequency link of an MV inverter, which mitigates the temperature increase occurring as a result of harmful harmonics by reducing the capacitive coupling at the high-frequency transformer. Four toroid core transformers with conventional and modified configurations, with 180° and 360° sector windings, were fabricated, and their THD, self-induced capacitance, and temperature were measured and compared. The transformer windings for all four

configurations were wound manually. The core material, dimensions, copper wire, and a number of winding turns were the same for the conventional and modified configuration, as listed in Table 3. The difference between the conventional and modified configuration was a two-part mold that was mounted over the secondary windings and ferrite core. The primary winding was then wound over this additional piece of hardware, which altered the dimensions of the primary winding and provided scope to unique winding arrangements. The mold was printed using a 3D printer with a PLA filament material. This was comprised of two parts, top and bottom, each with a width of 0.5 mm each with very negligible extra weight and cost [35,36].

3.1. Case 1: Conventional Toroid Core Transformer with 180° Sector Windings

In this configuration, the entire secondary winding is distributed over the 180° sector of the toroid core in a back-and-forth manner. The other half of the toroid core is wound with primary windings in a similar manner, as shown in Figure 5.
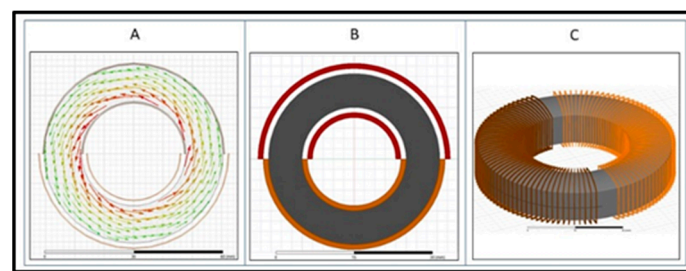

Figure 5. The 180° conventional (**A**) flux pattern in core; (**B**) 2D model; (**C**) 3D model.

3.2. Case 2: Modified Toroid Core Transformer with 180° Sector Windings

In this configuration, the secondary winding is distributed over the 180° sector of the toroid core in a back-and-forth manner, just as in the previous case. The two parts of the 3D printed mold using a PLA filament material were mounted over the ferrite toroid core and secondary windings, to completely encapsulate them. Owing to the assembly of the mold, the secondary winding is completely hidden, which leaves an entire 360° span for the primary winding. The initial experiments were carried out with the primary windings over the 360° sector and 180° sector of the core. On the other hand, the lowest leakage inductance was achieved when the primary had a 180° sector winding without overlapping the secondary winding, as shown in Figure 6.
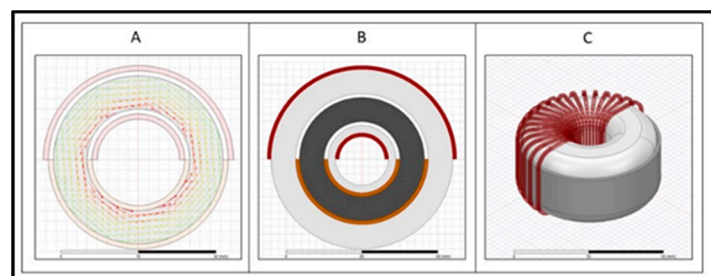

Figure 6. The 180° modified (**A**) flux pattern in core; (**B**) 2D model; (**C**) 3D model.

3.3. Case 3: A Conventional 360° Wound Toroid Core Transformer

In this case, the secondary winding is distributed over the entire 360° sector of the toroid ferrite core. The primary winding is also distributed over the 360° sector on top of the secondary winding (Figure 7).
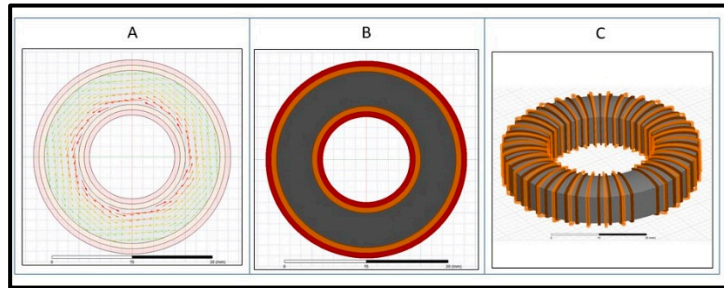
Figure 7. The 360° conventional (**A**) 2D model; (**B**) flux distribution; (**C**) 3D model.

3.4. Case 4: A Modified 360° Wound Toroid Core Transformer

In this case, the secondary winding is distributed over 360° sector of the toroid core in a back-and-forth manner, as in the former case. The toroid ferrite core along with the secondary winding is encapsulated with the 3D printed mold, over which the primary winding is wound around a 360° span (Figure 8).
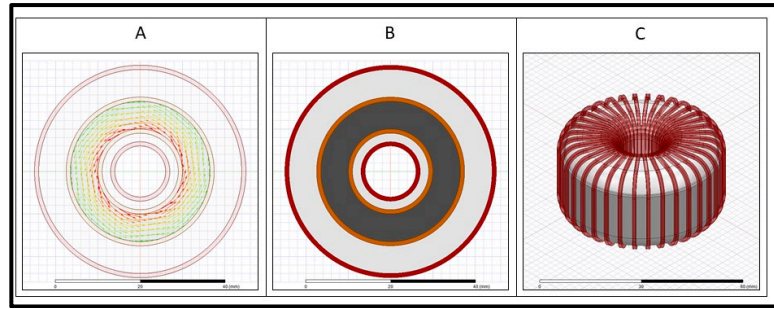

Figure 8. The 360° modified (**A**) 2D model; (**B**) flux distribution; (**C**) 3D model.

4. Calculation of the Transformer Inter-Winding Capacitance

The general structure (2D, 3D, and flux flow in core) of the four designed transformer's prototypes under test are illustrated in the fabrication section (3). In this section, prototype transformer calculations were carried out for inter-winding capacitance. Figure 9 shows the conceptual structure of case 1 and case 2 transformer prototypes for inter-winding capacitance calculation. Likewise, the capacitance for other prototypes can be evaluated in a similar manner.

Ferrite core material 77 has a negligible effect on parasitic capacitance; therefore, only winding configurations were taken into account. For the sake of simplicity, only one winding of the secondary side, which is wound on the ferrite core, is considered for calculation of inter-winding capacitance. The same position of the secondary winding is considered for all four cases.

The distance between the inner secondary winding and inner primary windings can be expressed as follows:

$$r_{1in,i} = \sqrt{r_1{}^2 + r_2{}^2 - 2r_1 r_2 \cos(\frac{\pi}{2} + \frac{\pi i}{n_p})} \tag{4}$$

where r_1 is the distance from the center of the core to the inner primary windings, r_2 is the distance from the center of the core to the outer primary windings, r_3 is the distance from the center of the core to the inner secondary windings, r_4 is the distance from the center of the core to the outer secondary windings (Figure 9), and n_p is the total number of primary turns. In all four cases, r_3 and r_4 values are the same, as secondary winding is wounded on the ferrite core and core dimension is same for all transformer prototypes. On the other hand, r_1 and r_2 values will vary with respect to each case, for example, r_1, for case 4 ($r_{1,4}$) and case 2 ($r_{1,2}$) will be same, but they are less than case 3 ($r_{1,3}$), which

in turn is less than case 1 ($r_{1,1}$). The details of r_1, r_2, r_3, r_4 for the four different configurations are given as follows:

$$A : r_{1,4} = r_{1,2} < r_{1,3} < r_{1,1}$$
$$B : r_{2,1} < r_{2,3} < r_{2,2} = r_{2,4}$$
$$C : r_{3,1} = r_{3,2} = r_{3,3} = r_{3,4}$$
$$D : r_{4,1} = r_{4,2} = r_{4,3} = r_{4,4}$$

The static capacitance between the inner primary and inner secondary is as follows:

$$C_{1in,i} = \frac{\in_\circ d\pi l_1}{2r_{1in,i}} = \frac{\in_\circ d\pi l_1}{2\sqrt{r_1^2 + r_2^2 - 2\,r_1 r_2 \cos(\frac{\pi}{2} + \frac{\pi i}{n_p})}} \tag{5}$$

where $\in_\circ$ is the permittivity of free space, d is the diameter of the wire used for primary and secondary windings, and l_1 is the overlapped length.

Assuming that the voltage potential distribution along the primary turn varies linearly,

$$V_p[i] = \frac{i}{n_p - 1} V_p \tag{6}$$

The total stored energy between the inner primary and secondary is as follows:

$$E_{1in} = \frac{1}{2} \sum_{i=0}^{n_p-1} \left(C_{1in,i} \left(\frac{i}{n_p - 1} V_p\right)^2 \right) \tag{7}$$

Similarly, the capacitance between the inner primary–outer secondary, outer primary–outer secondary, and outer primary–outer secondary can be calculated. Equations (4)–(7) can be used to find the capacitance and energy for the other three cases as well (Table 4). The simulation was run on MATLAB to calculate the capacitance in all four cases. For the sake of simplicity and to ignore the repetitive process of inter-winding capacitance calculations, only one winding in the same position of the secondary side is considered for all four cases. To see the effect of inter-winding capacitance, we choose three primary winding for 180° conventional and modified configurations instead of 116, and 6 primary windings for 360° conventional and modified configurations instead of 220.
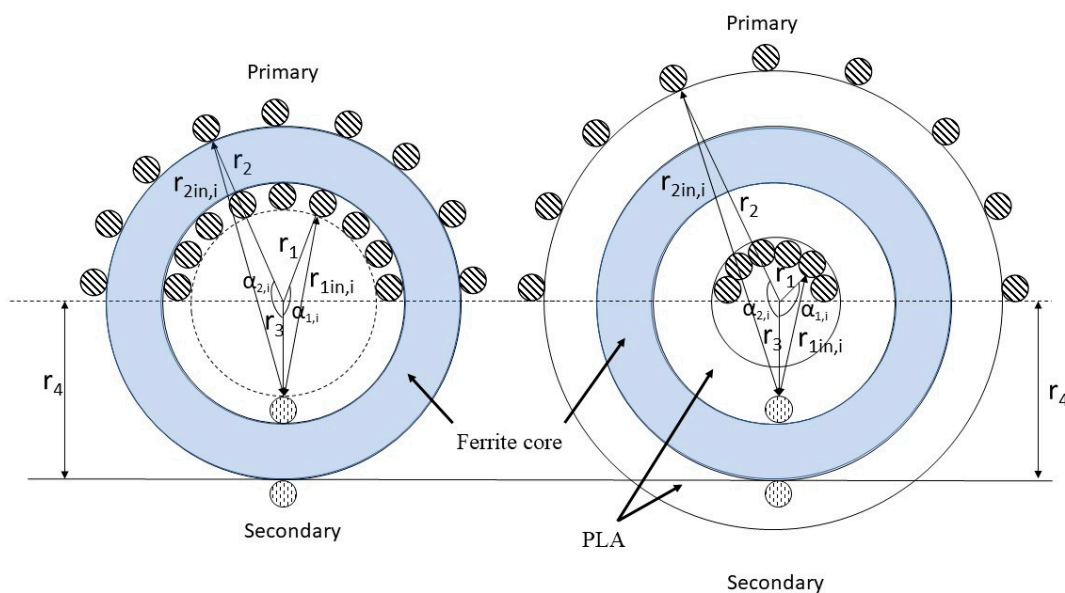

Figure 9. Toroidal transformer with 180° sectored winding, Conceptual presentation of transformer prototypes from left to right conventional and modified. PLA—polylactic acid.

Table 4. Detailed parameters of the transformer prototypes. PLA—polylactic acid.

Prototypes Physical Properties	Case 1	Case 2	Case 3	Case 4
Copper Wire standard	24 AWG	24 AWG	24 AWG	24 AWG
Primary Turns	116	116	220	220
Secondary Turns	116	116	220	220
Core Material (Table 1)	Ferrite 77	Ferrite 77	Ferrite77	Ferrite 77
Core shape	Ring	Ring	Ring	Ring
Permittivity (F/m)	8.85×10^{-12} (Air)	8.4190×10^{-12} (Air + PLA)	8.85×10^{-12} (Air)	8.419×10^{-12} (Air + PLA)
Inner Radius (mm)	17.775	15.275	17.775	15.275
Outer Radius (mm)	30.5	32.5	30.5	32.5
Primary Voltage (V)	24	24	24	24
Secondary Voltage (V)	~24	~24	~24	~24
Frequency (kHz)	1–30	1–30	1–30	1–30
r_1	17.265	14.765	16.755	14.765
r_2	30.5	32.5	31.01	32.5
r_3	17.265	17.265	17.265	17.265
r_4	30.5	30.5	30.5	30.5

It can be seen from Table 5 that the inter-winding capacitance would be highest for case 3, followed by that for case 1, case 4, and case 2. These analytical calculations hold well with the experimental data for inter-winding capacitance, which is shown in the next section.

Table 5. Theoratical analysis of all presented prototypes, calculated energy, and inter-winding capacitance.

	E_1	E_2	E_3	E_4	E_{total}	Capacitance$_{eq}$ (F)
Case 1						
Energy (J)	5.63×10^{-10}	3.87×10^{-10}	3.54×10^{-10}	2.87×10^{-10}	1.59×10^{-10}	2.76×10^{-12}
Percentage %	35.4	24.3	22.3	18	100	
Case 2						
Energy (J)	5.31×10^{-10}	3.74×10^{-10}	3.66×10^{-10}	2.94×10^{-10}	1.57×10^{-9}	2.72×10^{-12}
Percentage %	33.9	23.9	23.4	18.8	100	
Case 3						
Energy (J)	5.69×10^{-10}	3.87×10^{-10}	3.56×10^{-10}	2.90×10^{-10}	1.60×10^{-9}	2.78×10^{-12}
Percentage %	35.5	24.2	22.2	18.1	100	
Case 4						
Energy (J)	5.29×10^{-10}	3.73×10^{-10}	3.73×10^{-10}	3.00×10^{-10}	1.57×10^{-9}	2.73×10^{-12}
Percentage %	33.6	23.7	23.7	19	100	

5. Experimental Setup

The high-frequency transformer temperature, capacitive coupling, and leakage inductance were measured using a Fluke VT04A (Fluke, Everett, WA, USA) Thermometer and GWInstek LCR (GWINSTEK, New Taipei City, Tucheng Dist., Taiwan) meter. The experiments were conducted at constant ambient room temperature, on the high-frequency link of a 1 kW half bridge MV inverter. Two 38 V, 350 W standalone solar modules connected in parallel served as input for the developed inverter. Owing to the addition of a 3D printed mold and sector winding, it was possible to have different winding arrangements. A number of modified toroid high-frequency transformers have been developed with different sector windings, such as 45°, 90°, 120°, 180°, 270°, and 360°. Figure 10 presents a block diagram of the experimental setup. The input and output waveforms of the

transformer were stored, and the harmonic contents present in the waveform were analyzed by Matlab-FFT (MathWorks, Natick, MA, USA).
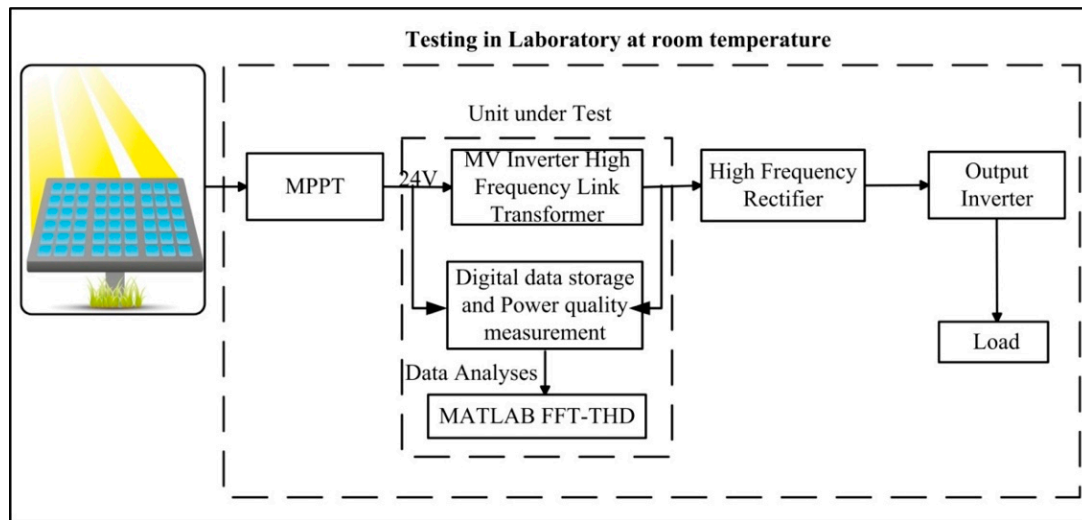

Figure 10. Block diagram for the testing process for prototypes PV high frequency based MV inverter systems. THD—total harmonics distortion.

6. Results and Discussion

For the comparative analysis, we designed a conventional toroid transformer with the same 180° and 360° sector windings and the same core dimension. The comparative experimental studies stated that the proposed modified design succeeded in lowering the inter-winding capacitance (approximately 87%) and controlling temperature increase issues (less than 30°) when compared with conventional designs; detailed discussion based on sectored winding is shown below. Table 6 compares the THD of the aforementioned transformer prototypes. By comparative analysis of normative Table 3 and experimental result Table 6, it is clearly visible that all the prototypes have a minimum risk. Although, modified designs have registered more or less similar distortion compared with conventional designs.

Table 6. Voltage and current THD for all prototypes.

Source Input Voltage (V)	Case	THD_V %		THD_I %	
		Primary	Secondary	Primary	Secondary
24	1	45.53	22.34	5.6	7.20
24	2	34.70	22.15	12.22	11.85
24	3	11.92	16.33	48.19	49.56
24	4	9.81	14.94	43.06	44.32

6.1. Toroidal Transformer with 180° Sectored Winding

Inter-winding Capacitance: Large inter-winding capacitance causes a significant amount of common mode noise at high-frequency operations. Figure 11 shows the comparison for parasitic capacitance from 1 to 30 kHz frequency at a high-frequency-based MV inverter. It is clearly visible that the proposed modified design has minimized the parasitic capacitance close to 20 pF, which is much lower than the conventional design. This was because of the mold, which helped increase the distance between the windings.
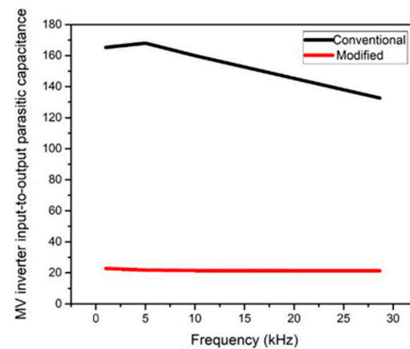
Figure 11. Toroidal transformers at 180° sectored winding, parasitic coupling capacitance comparison between the conventional and modified design of high-frequency link based MV inverter systems.

Leakage Inductance: In a sectored wound transformer, when the winding covers only 180°, leakage flux path changes in the core. According to theory, we expected the leakage inductance to be higher in modified design when compared with the conventional design because of the distance between windings created by the PLA mold. However, the 3D printed mold using PLA filament was mounted over the ferrite toroid core and secondary windings to completely encapsulate them and provided scope to increase the mean length turn of the primary winding, which is required to reduce the leakage inductance. This theory is supported by the experiment results [37]. Figure 12 demonstrates that the modified design recorded less leakage inductance than the conventional design.
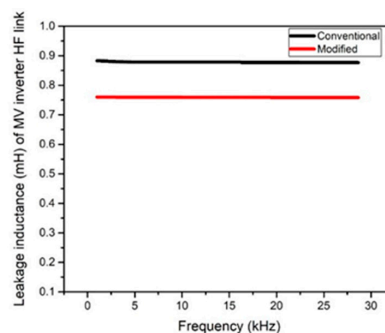

Figure 12. Toroidal transformers at 180° sectored winding, leakage inductance comparison between the conventional and modified design of high-frequency link based MV inverter systems.

Temperature: By comparing modified and conventional transformers on full load, it is clearly visible that lowering the interwinding capacitance and harmonics distortion helped significantly in controlling the temperature rise issue in the transformer (Figure 13).
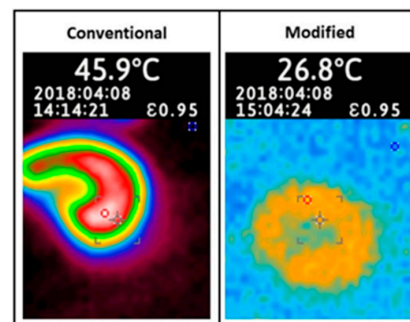

Figure 13. Toroidal transformers at 180° sectored winding, temperature comparison between the conventional and modified transformer design.

6.2. Toroidal Transformer with 360° Sectored Winding

The primary winding is on top of the secondary winding for the entire 360°, leakage flux is produced by the current in the windings, which are opposite in direction and equal in magnitude ($N_1 I_1 = N_2 I_2$), thus magnetizing or leakage flux cancels itself in the core.

Inter-winding Capacitance: Larger values of self-capacitance of the transformer, which occur between primary and secondary windings, play a vital role in large primary current distortions. Self-capacitance value of the proposed modified transformer prototype has been largely reduced (40 pF) with the help of 3D designed cover, spaces between windings, and proposed different winding arrangements compared with the conventional prototype. In Figure 14, winding capacitance for both conventional and modified transformers were plotted. It is noted that the modified design succeeded in minimizing the transformer self-capacitance by approximately 87% compared with conventional designs.
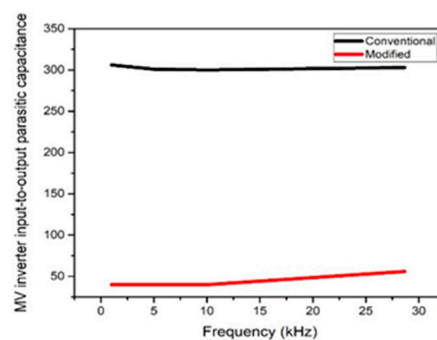

Figure 14. Toroidal transformers at 360° sectored winding, parasitic coupling capacitance comparison between the conventional and modified design of high-frequency link based MV inverter systems.

Leakage Inductance: The leakage inductance and primary/secondary capacitance are mutually exclusive and are governed by the distance between the windings and unwounded core. Therefore, it is difficult to achieve both low capacitive coupling and a high degree of inductive coupling in a power transformer. However, the magnetic core geometry and winding arrangements have a large influence on self-capacitance and leakage inductance of the transformer and because of the addition of a mold, it enables access to various types of winding arrangements. Thus, the modified design has successfully lowered the inter-winding capacitance and achieves the minimum difference between leakage inductance. The experimental results are shown in Figure 15.
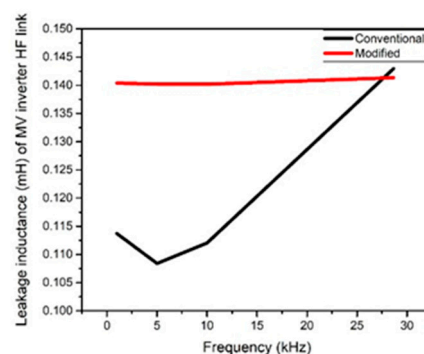

Figure 15. Toroidal transformers at 360° sectored winding, leakage inductance comparison of modified and conventional design of high-frequency link-based MV inverter systems.

Temperature: Modified design shows significant control in temperature rise by lowering the inter-winding capacitance and controlled leakage inductance over conventional designs (Figure 16).

An MV inverter high-frequency link-modified toroid transformer was designed differently from the conventional toroid designs. Both modified prototypes, case 2 and 4, showed extremely low coupling capacitance, that is, 20 pF and 40 pF, respectively. The toroidal transformer at 180° sectored winding has registered higher leakage inductance, which can be utilized in other topologies, such as dual active bridge topologies. The experimental results matched the calculated analysis quite well. Thus, the feasibility of the converter was validated.
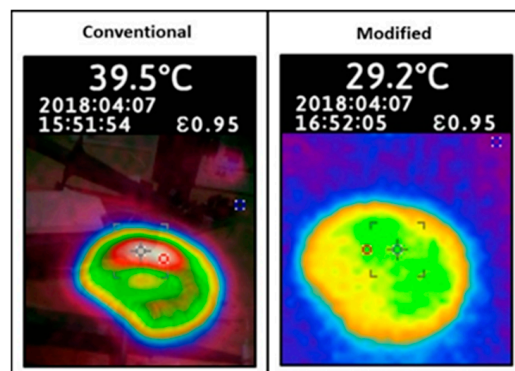

Figure 16. Toroidal transformers at 360° sectored winding, temperature comparison between the conventional and modified design of high-frequency link-based MV inverter systems.

7. Conclusions

Overall, the MV inverter with the proposed modified transformer design has a minimized total circuit input–output capacitance to approximately 20 pF, while the temperature increase was kept below 29.5 °C, without using any extra circuitry or cooling agent. The modified design is certainly a powerful solution to reduce the distortion in the waveform. This leads to an improved power quality of renewable power sources and an increase in the operational lifetime of the devices and loads involved in power systems. Hence, the MV inverter with the modified design transformer is more robust than other available power inverters of the same power rate. These experimental measurements, which agree with the mathematical derivation, prove that the transformer shape and winding arrangements have a huge impact on the inter-winding capacitance, and cannot be ignored in power inverters when power quality improvement is of concern.

Finally, the overall result achieved with the prototype provides a very high resistance to the common mode noise current caused by rapid voltage transients, which makes the MV inverter feasible for renewable energy sources applications. For future research, a study of the optimal design method on advanced prototypes with higher inductive coupling with more controlled THD will be conducted.

Author Contributions: H.-J.K., G.S.P., H.S., and H. conceptualized the idea of this research project. H.-J.K. and G.S.P. developed the proposal to the funding body. Finally, the project was awarded the funding. H., P.S., and H.S. discuss the design for the MV inverter high-frequency toroid transformer. H. and H.Y.L. developed the 3D design model including material selection. The fabrication and integration of the experimental setup were mostly carried out by the H., M.A.K. and M.U.A., under the supervision of H.J.K. and G.S.P. Mathematics derivation and real-time data was analyzed by H.S. and H. The paper was written by H. and H.J.K.

References

1. Gu, W.J.; Liu, R. A study of volume and weight vs. frequency for high-frequency transformers. In Proceedings of the IEEE Power Electronics Specialist Conference (PESC 1993), Seattle, WA, USA, 20–24 June 1993; pp. 1123–1129.
2. Leibl, M.; Ortiz, G.; Kolar, J.W. Design and experimental analysis of a medium-frequency transformer for solid-state transformer applications. *IEEE J. Emerg. Sel. Top. Power Electron.* **2017**, *5*, 110–123. [CrossRef]
3. Kulkarni, A.; John, V. New start-up scheme for HF transformer link photovoltaic inverter. *IEEE Trans. Ind. Appl.* **2017**, *53*, 232–241. [CrossRef]
4. Basu, K.; Mohan, N. A high-frequency link single-stage PWM inverter with common-mode voltage suppression and source-based commutation of leakage energy. *IEEE Trans. Power Electron.* **2014**, *29*, 3907–3918. [CrossRef]
5. De, D.; Ramanarayanan, V. A proportional $bm +$ multiresonant controller for three-phase four-wire high-frequency link inverter. *IEEE Trans. Power Electron.* **2010**, *25*, 899–906. [CrossRef]
6. Hayashi, Y.; Matsugaki, Y.; Ninomiya, T. Design Consideration for High Step-up Nonisolated Multicellular dc-dc Converter for PV Micro Converters. Available online: https://www.hindawi.com/journals/je/2018/5098083/ (accessed on 11 June 2018).
7. Kouro, S.; Leon, J.I.; Vinnikov, D.; Franquelo, L.G. Grid-connected photovoltaic systems: an overview of recent research and emerging PV converter technology. *IEEE Ind. Electron. Mag.* **2015**, *9*, 47–61. [CrossRef]
8. Sathishkumar, P.; Krishna, T.N.V.; Himanshu; Khan, M.A.; Zeb, K.; Kim, H.-J. Digital soft start implementation for minimizing start up transients in high power DAB-IBDC converter. *Energies* **2018**, *11*, 956. [CrossRef]
9. Alexander, S. Development of solar photovoltaic inverter with reduced harmonic distortions suitable for Indian sub-continent. *Renew. Sustain. Energy Rev.* **2016**, *56*, 694–704. [CrossRef]
10. Sathishkumar, P.; Himanshu; Piao, S.; Khan, M.A.; Kim, D.-H.; Kim, M.-S.; Jeong, D.-K.; Lee, C.; Kim, H.-J. A blended SPS-ESPS control DAB-IBDC converter for a standalone solar power system. *Energies* **2017**, *10*, 1431. [CrossRef]
11. Singh, R.; Taghizadeh, S.; Tan, N.M.L.; Pasupuleti, J. Battery energy storage system for PV output power leveling. *J. Eng.* **2018**, *2018*, 5098083. Available online: https://www.hindawi.com/journals/ape/2014/796708/ (accessed on 11 June 2018). [CrossRef]
12. Bolduc, P.; Lehmicke, D.; Smith, J. Performance of a grid-connected PV system with energy storage. In Proceedings of the 23th IEEE Photovoltaic Specialists Conference (Cat. No.93CH3283-9), Louisville, KY, USA, 10–14 May 1993; pp. 1159–1162.
13. Tan, N.M.L.; Abe, T.; Akagi, H. Design and performance of a bidirectional isolated DC–DC converter for a battery energy storage system. *IEEE Trans. Power Electron.* **2012**, *27*, 1237–1248. [CrossRef]
14. McBee, K.D. Transformer aging due to high penetrations of PV, EV charging, and energy storage applications. In Proceedings of the 2017 Ninth Annual IEEE Green Technologies Conference (GreenTech), Denver, CO, USA, 29–31 March 2017; pp. 163–170.
15. Bojoi, R.I.; Limongi, L.R.; Roiu, D.; Tenconi, A. Enhanced power quality control strategy for single-phase inverters in distributed generation systems. *IEEE Trans. Power Electron.* **2011**, *26*, 798–806. [CrossRef]
16. Eltawil, M.A.; Zhao, Z. Grid-connected photovoltaic power systems: Technical and potential problems—A review. *Renew. Sustain. Energy Rev.* **2010**, *14*, 112–129. [CrossRef]
17. Popavath, L.N.; Kaliannan, P. Photovoltaic-STATCOM with Low Voltage Ride through Strategy and Power Quality Enhancement in a Grid Integrated Wind-PV System. *Electronics* **2018**, *7*, 51. [CrossRef]
18. Real-Calvo, R.; Moreno-Munoz, A.; Gonzalez-De-La-Rosa, J.J.; Pallares-Lopez, V.; Gonzalez-Redondo, M.J.; Moreno-Garcia, I.M. An embedded system in smart inverters for power quality and safety functionality. *Energies* **2016**, *9*, 219. [CrossRef]
19. Li, Y.; Oruganti, R. A flyback-CCM inverter scheme for photovoltaic AC module application. *Aust. J. Electr. Electron. Eng.* **2009**, *6*, 301–309. [CrossRef]
20. Pairodamonchai, P.; Suwankawin, S.; Sangwongwanich, S. Design and implementation of a hybrid output EMI filter for high-frequency common-mode voltage compensation in PWM inverters. *IEEE Trans. Ind. Appl.* **2009**, *45*, 1647–1659. [CrossRef]

21. Wang, F.; Duarte, J.L.; Hendrix, M.A.M.; Ribeiro, P.F. Modeling and analysis of grid harmonic distortion impact of aggregated DG inverters. *IEEE Trans. Power Electron.* **2011**, *26*, 786–797. [CrossRef]

22. Grady, W.M.; Santoso, S. Understanding power system hannonics. *IEEE Power Eng. Rev.* **2001**, *21*, 8–11. [CrossRef]

23. Abdi, B.; Ranjbar, A.H.; Farabi, V.; Yazdanparast, M.S. Effect of transformer's parameters on harmonic generation. *Energy Procedia* **2011**, *12*, 679–685. [CrossRef]

24. Murthy-Bellur, D.; Kazimierczuk, M.K. Winding losses caused by harmonics in high-frequency flyback transformers for pulse-width modulated dc-dc converters in discontinuous conduction mode. *IET Power Electron.* **2010**, *3*, 804–817. [CrossRef]

25. Zolfaghari, A.; Chan, A.; Razavi, B. Stacked inductors and transformers in CMOS technology. *IEEE J. Solid-State Circuits* **2001**, *36*, 620–628. [CrossRef]

26. Portolan, A.; Hofsajer, I.W. The analysis and design of an inter-winding shielding structure of a high frequency transformer. In Proceedings of the 2007 IEEE Power Engineering Society Conference and Exposition in Africa-PowerAfrica, Johannesburg, South Africa, 16–20 July 2007; pp. 1–6.

27. Nguyen-Duy, K.; Ouyang, Z.; Knott, A.; Andersen, M.A.E. Minimization of the transformer inter-winding parasitic capacitance for modular stacking power supply applications. In Proceedings of the 2014 16th IEEE European Conference on Power Electronics and Applications, Lappeenranta, Finland, 26–28 August 2014; pp. 1–10.

28. Ali, M.U.; Nengroo, S.H.; Khan, M.A.; Zeb, K.; Kamran, M.A.; Kim, H.J. A real-time simulink interfaced fast-charging methodology of lithium-ion batteries under temperature feedback with fuzzy logic control. *Energies* **2018**, *11*, 1122.

29. Ajami, A.; Farakhor, A.; Ardi, H. Minimisations of total harmonic distortion in cascaded transformers multilevel inverter by modifying turn ratios of the transformers and input voltage regulation. *IET Power Electron.* **2014**, *7*, 2687–2694. [CrossRef]

30. Kashyap, M.; Kansal, S. Temperature control in transformer using intelligent system. In Proceedings of the 2015 2nd IEEE International Conference on Recent Advances in Engineering Computational Sciences (RAECS), Chandigarh, India, 21–22 December 2015; pp. 1–6.

31. Hurezeanu, I.; Nicola, C.I.; Sacerdoţianu, D.; Nicola, M.; Aciu, A.M.; Niţu, M.C. Temperature control and monitoring system for power transformer windings using fiber optic sensors. In Proceedings of the 2016 IEEE International Symposium on Fundamentals of Electrical Engineering (ISFEE), Bucharest, Romania, 30 June–2 July 2016; pp. 1–4.

32. Blache, F.; Keradec, J.P.; Cogitore, B. Stray capacitances of two winding transformers: equivalent circuit, measurements, calculation and lowering. In Proceedings of the 1994 IEEE Industry Applications Society Annual Meeting, Denver, CO, USA, 2–6 October 1994; pp. 1211–1217.

33. Conway, D.W. Shielded Electrical Wire Construction, and Transformer Utilizing the same for Reduction of Capacitive Coupling. U.S. Patent 5,012,125, 30 April 1991.

34. De León, F.; Purushothaman, S.; Qaseer, L. Leakage inductance design of toroidal transformers by sector winding. *IEEE Trans. Power Electron.* **2014**, *29*, 473–480. [CrossRef]

35. Mathew, A.P.; Oksman, K.; Sain, M. Mechanical properties of biodegradable composites from poly lactic acid (PLA) and microcrystalline cellulose (MCC). *J. Appl. Polym. Sci.* **2005**, *97*, 2014–2025. [CrossRef]

36. Silverajah, V.S.G.; Ibrahim, N.A.; Zainuddin, N.; Yunus, W.M.Z.W.; Hassan, H.A. Mechanical, thermal and morphological properties of poly (lactic acid)/epoxidized palm olein blend. *Molecules* **2012**, *17*, 11729–11747. [CrossRef] [PubMed]

37. Mclyman, C.W. *Transformer and Inductor Design Handbook*; CRC Press: Boca Raton, FL, USA, 2004. Available online: https://www.taylorfrancis.com/books/9780203913598 (accessed on 31 March 2004).